Research Article Vol. 13, No. 11 / 1 Nov 2023 / Optical Materials Express 3342

Optical Materials EXPRESS

Enhanced hole injection in Ga-polar 290 nm AlGaN-based DUV LEDs with a p-n junction hole accelerator

WENTAO TIAN,[1,2] **MENGRAN LIU,**[1,2] **SHUTI LI,**[3] **AND CHAO LIU**[1,2,*]

[1] *School of Microelectronics, Institute of Novel Semiconductors, Shandong Technology Center of Nanodevices and Integration, State Key Laboratory of Crystal Materials, Shandong University, Jinan 250100, China*
[2] *Shenzhen Research Institute, Shandong University, Shenzhen 518057, China*
[3] *Guangdong Engineering Research Center of Optoelectronic Functional Materials and Devices, Institute of Semiconductors, South China Normal University, Guangzhou, 510631, China*
[*] *chao.liu@sdu.edu.cn*

Abstract: The limited kinetic energy of holes in AlGaN-based deep ultraviolet light-emitting diodes (DUV LEDs) poses a challenge in their transportation into the active region across the Al-rich electron blocking layer (EBL) and significantly restricts the electrical and optical performance of DUV LEDs. In this work, we propose a hole accelerator structure composing a p-$Al_xGa_{1-x}N$/n-$Al_xGa_{1-x}N$ junction to improve the hole injection efficiency and explore the mechanism behind the enhanced performance with the Advanced Physical Models of Semiconductor Devices software (APSYS). The built-in electric field of the p-n junction distributes along the [000-1] direction, which can enhance the hole drift velocity and improve the hole injection into the active region. Moreover, with an optimum Al composition of 50%, [000-1] oriented polarization-induced electric field can be generated at the vicinity of both the p-EBL/accelerator and accelerator/hole supplier interfaces, which further boosts the holes into the active region. Besides, the original steep barrier for holes at the EBL/hole supplier interface can be splited into a two-step barrier which is more favorable for hole transportation. As a result, an enhanced optical power by 49.4% and alleviated efficiency droop by 76.3% can be achieved with the proposed p-n junction-based hole accelerator. The results can pave the way for AlGaN-based DUV LEDs towards high-power and high-efficiency applications.

1. Introduction

Compared with conventional mercury-based lamps, AlGaN-based deep ultraviolet light-emitting diodes (DUV LEDs) exhibit distinctive characteristics, including compact form factor, diminished power consumption, and prolonged operational longevity [1–4]. These features position them as prospective light sources in the realm of transportation, communication, and disinfection [5–8]. Over the past decade, extensive research has been devoted to enhancing the crystalline quality and improving the epitaxial structure of DUV LEDs, with the aim of achieving high-performance AlGaN-based DUV LEDs [9–13]. However, the external quantum efficiency (EQE) of DUV LEDs still remains below 10% and features severe droop behavior under high injection current density, thereby constraining the widespread commercial deployment of AlGaN-based DUV LEDs [14–17].

It has been indicated that the severe electron leakage and insufficient hole injection are two key issues among the factors impeding the improvement of device performance [18,19]. To suppress the electron leakage, numerous approaches have been put forward from the following aspects, such as adopting an electron cooler (EC) in the n-type region to weaken the kinetic energy of

#502136 https://doi.org/10.1364/OME.502136
Journal © 2023 Received 31 Jul 2023; revised 19 Sep 2023; accepted 23 Sep 2023; published 30 Oct 2023

electrons [20], employing a streamlined quantum barrier to enhance the ratio of electron capture in the active region [21], and introducing an Al-rich electron blocking layer (EBL) between the last quantum barrier (LQB) and p-AlGaN hole supplier to prevent the electrons from overflying into the p-type region [22]. Thereinto, the utilization of p-type EBL structure with high Al component has gained widespread commercial application. However, the Al-rich EBL structure tends to result in insufficient hole injection efficiency, which can be ascribed to the hole depletion caused by the positive sheet charges at the LQB/EBL interface and the hole blocking effect induced by the large potential barrier in the valence band of EBL [23–25]. Thus, it is imperative to explore effective approaches to enhance hole injection into the multiple quantum well (MQW) region.

Various structures have emerged to ameliorate hole depletion in the proximity of the LQB/EBL interface [26,27]. Specifically, AlN layer [28], AlGaN/AlGaN superlattice [29–31], and AlGaN layer [32] has been inserted between LQB and EBL to convert the positive sheet charges into the negative sheet charges at the LQB/EBL interface, which can promote the hole injection into the active region. In order to mitigate hole blocking effect induced by the large potential barrier in the valence band of EBL, numerous energy band engineering strategies of the EBL structure has been suggested, such as p-AlInN EBL [33], step-graded superlattice EBL [34,35], taper-shaped EBL [36], and graded ud-AlGaN EBL [37]. Except for the aforementioned approaches to enhance hole injection efficiency, energizing holes via increasing their velocity is another practical strategy to bolster hole transportation from the p-type layer into the active region. Reference [38] reported the existence of polarization-induced electric field oriented along the [000-1] direction between EBL and p-AlGaN hole supplier, as well as between p-AlGaN hole supplier and p-GaN hole supplier, which can enhance the drift velocity of holes and thus boosting the hole injection into the active region. The [000-1] oriented electric field at the p-AlGaN/p-GaN interface has been utilized to enhance the hole injection by Zhang et al [39] and proved to be effective in enhancing the optical performance of DUV LEDs. However, the exploration of accelerating holes through modulating the electric field at the vicinity of the p-EBL/p-AlGaN interface remains an uncharted territory in current research.

In this work, we propose a p-n junction based hole accelerator that consists of a p-$Al_xGa_{1-x}N$/n-$Al_xGa_{1-x}N$ structure for the purpose of enhancing the hole injection efficiency and improving the optical performance of DUV LEDs. The ionized donor-acceptor pairs within the p-$Al_xGa_{1-x}N$/n-$Al_xGa_{1-x}N$ structure give rise to a [000-1] oriented built-in electric field between the EBL and p-AlGaN hole supplier, effectively enhancing the kinetic energy of holes and improving the probability of holes being injected into the active region. Besides, the polarization-induced electric field at the both side of the p-n junction based hole accelerator also distributes along the [000-1] direction, which can further bolster the hole injection efficiency of DUV LEDs. Moreover, through the optimization of Al component in the p-n junction, the valence band offset between EBL and p-AlGaN hole supplier in proposed devices can be significantly ameliorated compared to the reference device. Consequently, the proposed device with p-$Al_{0.5}Ga_{0.5}N$/n-$Al_{0.5}Ga_{0.5}N$ structure possesses the largest accelerating electric field and the smallest barrier height at the EBL/p-AlGaN interface among the investigated devices, leading to an enhancement in the optical power by 49.4% and a reduction in the efficiency droop by 76.3% at an injection current density of 150 A/cm^2. Therefore, the redesigned device with a p-n junction based hole accelerator provides an effective strategy to achieve AlGaN-based DUV LEDs with high photoelectric property.

2. Device structure and parameters

To investigate the effects of the hole accelerator on the device performance of DUV LEDs, two types of AlGaN-based DUV LEDs (i.e., Device A with conventional structure and Device i with p-$Al_xGa_{1-x}N$/n-$Al_xGa_{1-x}N$ structure) are designed, as presented in Fig. 1. The reference structure (Device A) from Ref. [40] is initiated with a 4-μm-thick n-$Al_{0.6}Ga_{0.4}N$ layer, whose effective electron concentration is 8×10^{18} cm^{-3}. The active region with 5 pairs of 3-nm-thick $Al_{0.45}Ga_{0.55}N$ quantum well (QW) and 10-nm-thick $Al_{0.57}Ga_{0.43}N$ quantum barrier (QB) are stacked in sequence. A 10-nm-thick $Al_{0.6}Ga_{0.4}N$ electron blocking layer is set on the top of the MQW region to prevent electrons in the active region from overflowing into p-type region. Afterwards, a 50-nm-thick p-$Al_{0.4}Ga_{0.6}N$/50-nm-thickness p-GaN heterojunction is appointed as the hole supplier, in which the effective hole concentration is set to be $\sim 1 \times 10^{17}$ cm^{-3}. In regards to the proposed devices (Device B, C, and D, as shown in Fig. 1(c)), they possess identical epitaxial structures except that a p-$Al_xGa_{1-x}N$/n-$Al_xGa_{1-x}N$ structure with tunable Al composition ($x = 0.4$, $x = 0.5$, $x = 0.6$) is introduced between the EBL and p-AlGaN hole supplier. The doping concentration of the n-$Al_xGa_{1-x}N$/p-$Al_xGa_{1-x}N$ insertion layer is set to be 2×10^{17} cm^{-3} (N_D) and 4×10^{17} cm^{-3} (N_A), respectively. The mesa sizes of epitaxial structures are set to be 350 µm × 350 µm.

As shown in Fig. 1(b), a [000-1] oriented polarization-induced electric field (E_p) arises at the EBL/p-AlGaN hetero-interface of the conventional DUV LED structure, which is induced by the lattice mismatch between the p-EBL and the p-AlGaN layer. The local E_p can accelerate holes and the net work (denoted as W_i) done to the holes via E_p is calculated by

$$W_i(x) = q \int_0^L E_p dx, \tag{1}$$

where q represents the elementary charge, and L is the length of p-AlGaN hole supplier.

As for the proposed structures with embedded p-AlGaN/n-AlGaN junction shown in Fig. 1(c), the ionized donors and acceptors in the PN junction create an additional built-in electric field (E_b), which adds to the intrinsic polarization-induced electric fields (E_{pp}) at the p-EBL/p-$Al_xGa_{1-x}N$ and n-$Al_xGa_{1-x}N$/p-AlGaN hole supplier interfaces.

The kinetic energy obtained by holes from the composite electric field above is expressed as

$$W_i(x) = q \int_0^{T+L} E_{pp} dx + q \int_0^T E_b dx, \tag{2}$$

where T is the thickness of p-$Al_xGa_{1-x}N$/n-$Al_xGa_{1-x}N$ structure, and L is the length of p-AlGaN hole supplier. The ionized donor-acceptor pairs within p-$Al_xGa_{1-x}N$/n-$Al_xGa_{1-x}N$ junction (J_0) and n-$Al_xGa_{1-x}N$/p-AlGaN junction (J_1) result in [000-1] oriented built-in electric field and [0001] oriented built-in electric field, respectively. The depletion region width (W_{DR}) of p-$Al_xGa_{1-x}N$/n-$Al_xGa_{1-x}N$ junction (J_0) and n-$Al_xGa_{1-x}N$/p-$Al_{0.4}Ga_{0.6}N$ junction (J_1) is calculated by

$$W_{DR} = \sqrt{\frac{2\varepsilon_r\varepsilon_0}{q}\left(\frac{N_A + N_D}{N_A N_D}\right)V_{bi}}, \tag{3}$$

in which the ε_r and V_{bi} are relative dielectric constant of $Al_xGa_{1-x}N$ alloy and built-in potential in the p-$Al_xGa_{1-x}N$/n-$Al_xGa_{1-x}N$, respectively. The ε_r and $V_{bi_{Al_xGa_{1-x}N}}$ can be obtained by

$$\varepsilon_{r_{Al_xGa_{1-x}N}} = x\varepsilon_{r_{AlN}} + (1-x)\varepsilon_{r_{GaN}}, \tag{4}$$

$$V_{bi} = \frac{k_B T}{q} \ln\left(\frac{N_A N_D}{n_i^2}\right), \tag{5}$$

where $\varepsilon_{r_{AlN}}$, $\varepsilon_{r_{GaN}}$ are relative dielectric constant of AlN and GaN respectively and can be found in Ref. [41]. The equilibrium carrier concentration of $Al_xGa_{1-x}N$ alloy is defined as according

Optical Materials EXPRESS

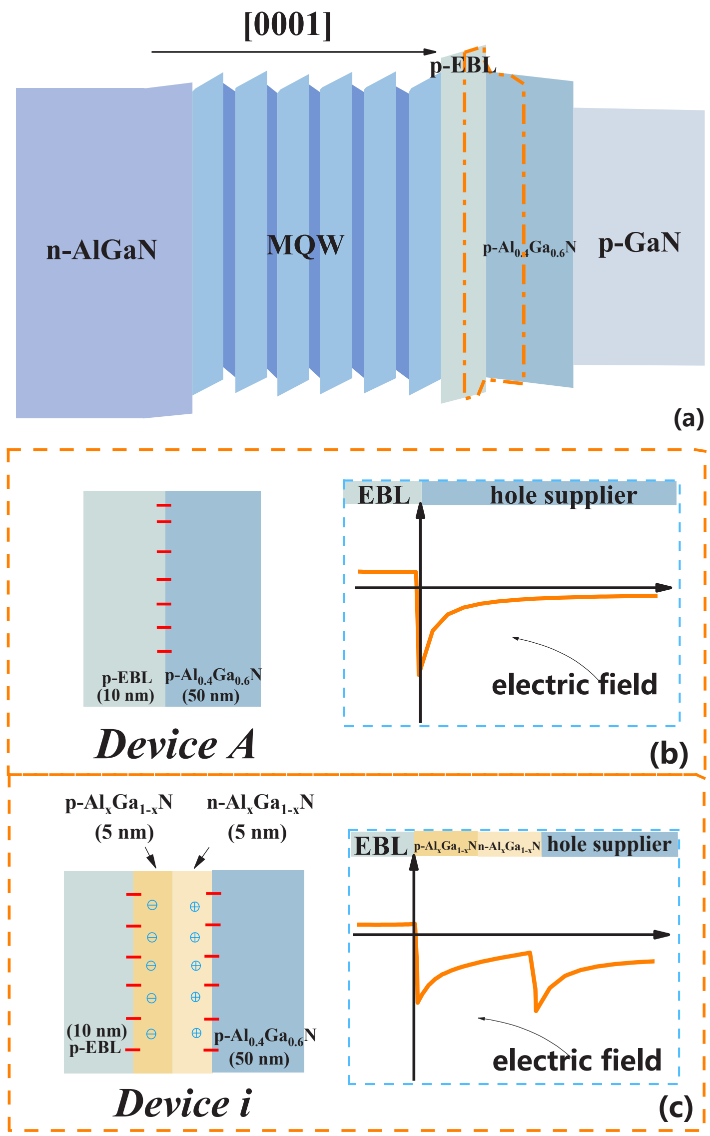

Fig. 1. (a) Estimated energy band diagram of the investigated AlGaN-based DUV LEDs. Structure diagram and electric field between p-EBL and part of p-AlGaN hole supplier for the (b) reference device and (c) proposed devices, respectively.

Optical Materials EXPRESS

Ref. [42]

$$n_i = \sqrt{4\left(\frac{k_B}{2\pi\hbar^2}\right)^3 (m^*_{e_{AlGaN}} * m^*_{h_{AlGaN}})^{\frac{3}{2}} T^3 e^{-\frac{E_{g\_AlGaN}}{k_B T}}} \tag{6}$$

Besides, for $Al_xGa_{1-x}N$ alloy, the effective mass of electrons is obtained by utilizing

$$m^*_{e_{Al_xGa_{1-x}N}} = x m_{e_{AlN}} + (1-x) m_{e_{GaN}}, \tag{7}$$

in which the effective mass of electrons of AlN and GaN are assumed $m_{e_{AlN}} = 0.48 m_0$, $m_{e_{GaN}} = 0.22 m_0$. Similarly, the effective mass of holes can be derived from

$$m_{h_{Al_xGa_{1-x}N}} = x m_{h\_AlN} + (1-x) m_{h_{GaN}}, \tag{8}$$

where the effective mass of holes of AlN and GaN is $m_{h_{AlN}} = 0.7 m_0$, $m_{h_{GaN}} = 0.4 m_0$ [43,44]. Consequently, the depletion region widths in Device B, Device C, and Device D are 176.11 nm, 180.49 nm, and 184.72 nm, respectively, provided that p-$Al_xGa_{1-x}N$, n-$Al_xGa_{1-x}N$, and p-AlGaN layer have infinite thicknesses [45]. Thus, the p-n junction based hole accelerator insertion layer, which comprises 5-nm-thickness p-$Al_xGa_{1-x}N$ layer and 5-nm-thickness n-$Al_xGa_{1-x}N$ layer, is completely depleted. Besides, please note that the J_0 is reverse biased and the J_1 is forward biased under forward conduction condition. With the increased applied voltage, the depletion region of J_1 is narrowed, while that of J_0 can be extended to the overall p-$Al_xGa_{1-x}N$/n-$Al_xGa_{1-x}N$ structure. Thus, the dominant role in accelerating holes is played by the built-in electric field that distributes along the [000-1] orientation. Therefore, the net work done to holes via the composite electric field in the proposed structures with p-n junction hole accelerator is

$$W_i(x) = q\int_0^{T+L} E_p dx + q\int_0^{L} E_p dx + \int_0^{T/2} \frac{qN_A l}{\varepsilon_r \varepsilon_0} q dl + \int_0^{T/2} \frac{qN_D l}{\varepsilon_r \varepsilon_0} q dl. \tag{9}$$

To explore the optical and electrical characteristics of the AlGaN-based DUV LEDs with the proposed p-n junction hole accelerator, we conducted numerical calculations via utilizing Advanced Physical Models of Semiconductor Devices (APSYS) software, which can manage material parameters, Schrödinger equation, Poisson's equation, current continuity equation, drift-diffusion equation for III-nitride semiconductors [46]. The light extraction efficiency (LEE), the energy band offset ratio for AlGaN/AlGaN heterojunction, and the polarization level are set to be 6%, 50:50, and 40%, respectively. Besides, the nonradiative recombination parameters in the active region, such as the Shockley-Read-Hall (SRH) recombination lifetime, and Auger recombination coefficient, and light extraction efficiency, are set to be 14 ns, 1.7×10^{-30} cm^6/s, and 6%, respectively. The intraband tunneling model [47] and non-local quantum well (QW) transport model [48] also play a key role in the calculation module. Additionally, we extracted both experimental measurement results and the calculated value of optical power and EQE for Device A at the different injection current density, as depicted in Fig. 2. It is evident that the calculation values align well with the experimental results, which is attributed to the effective parameters employed in the calculation model.

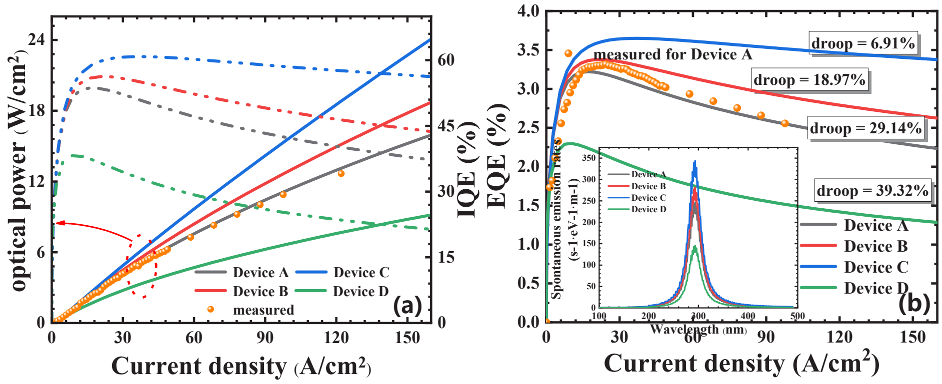

Fig. 2. (a) Calculated optical power, IQE and (b) EQE in term of the injected current density for Device A, B, C, and D, respectively. The label in Fig. 2(b) displays the value of efficiency droop for the investigated devices. Measured EQE and optical power for Device A are also presented. The inset of Fig. 2(b) presents the spontaneous emission intensity of the investigated devices.

3. Results and discussion

For the purpose of exploring the effects of the p-$Al_xGa_{1-x}N$/n-$Al_xGa_{1-x}N$ structure on the device performance, the light optical power (LOP) and internal quantum efficiency (IQE) of the investigated devices were analyzed as a function of the injection current density and depicted in Fig. 2(a). The EQE (η_{EQE}) is displayed in Fig. 2(b) and calculated by the formula [49] shown below

$$\eta_{EQE} = \eta_{IQE} \times \eta_{extr}, \tag{10}$$

in which η_{IQE} is the internal quantum efficiency, and η_{extr} is the light extraction efficiency. The efficiency droop is calculated by the following equation to evaluate the degree of EQE degradation with increased injection current density:

$$efficiency\ droop = \frac{EQE_{max} - EQE_J}{EQE_{max}} \tag{11}$$

in which EQE_{max} and EQE_J represent the peak value of the EQE and the EQE value at the injection current density of J, respectively. Compared with Device A, Device B with p-$Al_{0.4}Ga_{0.6}N$/n-$Al_{0.4}Ga_{0.6}N$ structure exhibits a 21.81% increase in the optical power at a current density of 150 A/cm^2. The efficiency droop is reduced from 29.14% in Device A with conventional structure to 18.97% in Device B with an p-$Al_{0.5}Ga_{0.5}N$/n-$Al_{0.5}Ga_{0.5}N$ structure. As for Device C featuring a p-$Al_{0.5}Ga_{0.5}$/n-$Al_{0.5}Ga_{0.5}N$ structure, the optical power is further increased by 49.40% at a current density of 150 A/cm^2. It can be observed that Device C possess the lowest efficiency droop of 6.91% among the proposed devices at an injection current density of 150 A/cm^2. However, as the AlN component in the insertion layer increases, Device D with p-$Al_{0.6}Ga_{0.4}N$/n-$Al_{0.6}Ga_{0.4}N$ structure exhibits the lowest EQE and optical power among the investigated devices. The emission curves of the investigated devices are displayed in the inset of Fig. 2(b). It can be observed that there is no difference in the peak wavelength (290 nm) between the reference and proposed devices. The peak value of the emission curves follows the same tendency as LOP of the investigated devices.

To elaborate the inherent mechanism behind the diverse device performance, we constructed energy band diagrams coupled with the electric field from LQB to p-AlGaN hole supplier for the investigated devices, as depicted in Fig. 3(a-d). These figures also illustrate the presence

Optical Materials EXPRESS

of polarization-related charges (denoted as σ_0, σ_1, and σ_2) between EBL and p-AlGaN hole supplier. Additionally, the Φ_C, Φ_H, ΔE, and W_i represent the effective barrier height for electrons, the effective barrier height for holes, the energy barrier/valence band offset between EBL and p-AlGaN hole supplier, and the net work done to holes by the electric field between EBL and p-$Al_{0.4}Ga_{0.6}N$, respectively. Table 1 presents the values of Φ_C, Φ_H, ΔE, and W_i for the investigated devices. Furthermore, to further explore the impact of the p-Al_xGa_{1-x}/n-$Al_xGa_{1-x}N$ structure on hole injection, the hole concentration between EBL and part of the p-AlGaN hole supplier is displayed in Fig. 3(e).

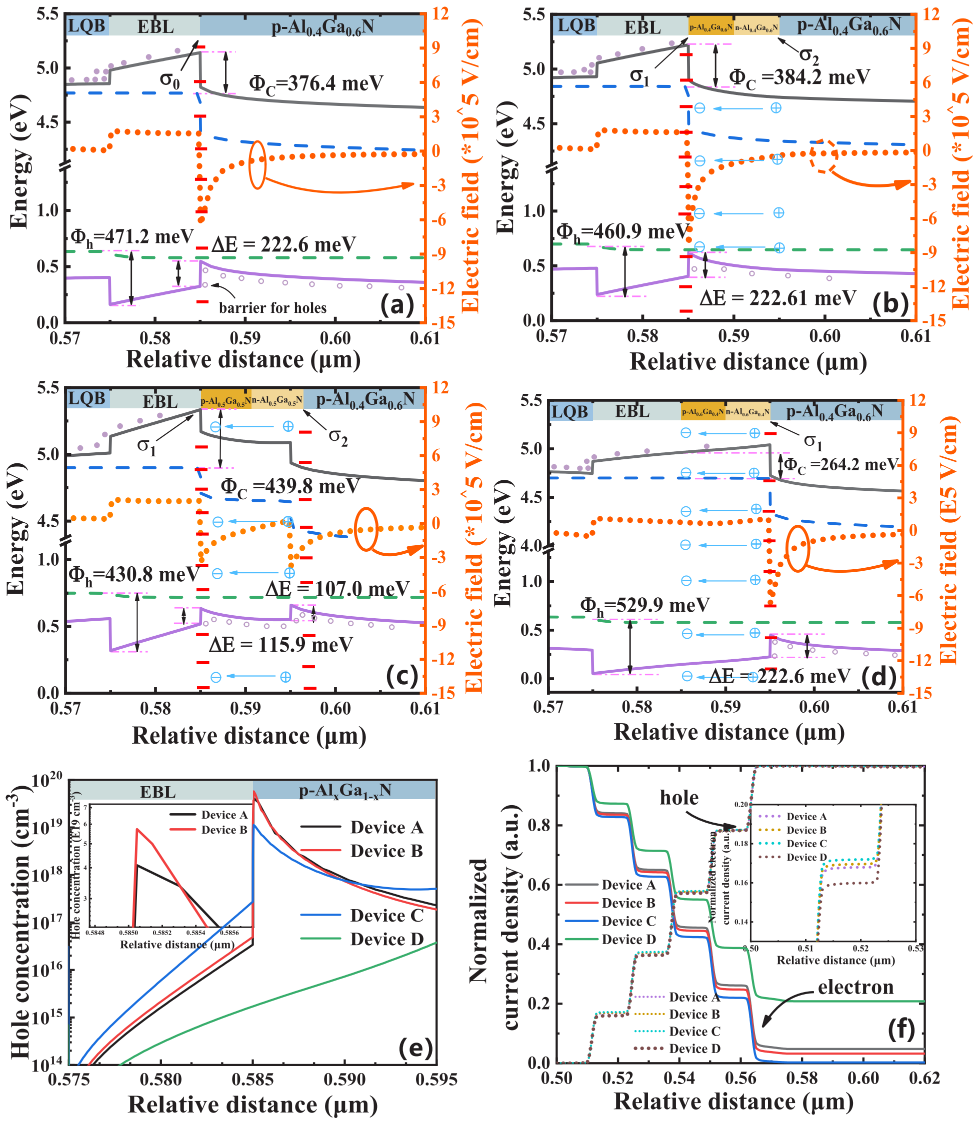

Fig. 3. Energy band and electric field diagrams of (a) Device A (b) Device B (c) Device C (d) Device D. The value of electric field is defined as positive subject to the [0001] oriented direction, and vice versa. (e) Hole concentration between EBL and part of p-AlGaN hole supplier. (f) Normalized electron and hole current density for all devices at an injection current density of 150 A/cm^2

Optical Materials EXPRESS

Table 1. the work done to holes by the electric field (W_i), the barrier height between EBL and p-AlGAaN layer (ΔE), the effective barrier height for electrons (Φ_C), the effective barrier height for holes (Φ_H)

	Device A	Device B	Device C	Device D
W_i	336.6 meV	338.1 meV	388.5 meV	261.8 meV
ΔE	222.6 meV	222.6 meV	115.9 meV/107.0 meV	0/222.6 meV
Φ_C	376.4 meV	384.2 meV	439.8 meV	264.2 meV
Φ_H	471.2 meV	460.9 meV	430.8 meV	529.9 meV

As for Device A with conventional structure, holes are able to acquire a kinetic energy of 336.6 meV through the polarization-induced electric field (E_p) while traveling from the p-type hole supplier towards the EBL/p-AlGaN interface. However, there exists a large potential barrier of 222.6 meV (ΔE) at the EBL/p-AlGaN interface due to the severe Al composition discontinuity between EBL and p-AlGaN hole supplier, as shown in Fig. 3(a). After being injected into the EBL, the holes in the vicinity of EBL/p-AlGaN interface experience an energy loss equivalent to ΔE. The restricted kinetic energy makes it difficult for holes to be injected into the active region across the large effective valence band barrier ($\Phi_H = 471.2$ meV) of EBL, resulting in an insufficient hole injection efficiency for Device A.

In comparison with Device A, the holes in Device B can obtain a larger kinetic energy ($W_B = 338.1$ meV) thanks to the incorporation of an additional built-in electric field (E_b) by the inserted p-n junction. Besides, the effective valence band barrier height for holes at the EBL is reduced from 471.2 meV in Device A to 460.9 meV in Device B, further facilitating the transportation of holes into the active region. However, despite the enhanced kinetic energy, part of holes still encounters hindrance from the large potential barrier at the EBL/p-$Al_{0.4}Ga_{0.6}N$ interface. As shown in the inset of Fig. 3(e), Device B exhibits a higher hole concentration in the vicinity of the EBL/p-$Al_{0.4}Ga_{0.6}N$ interface than Device A. It is indicated that the effect of the p-n junction hole accelerator on the enhanced hole injection efficiency is constrained by the large potential barrier at the EBL/p-$Al_{0.4}Ga_{0.6}$ interface, leading to a slightly higher hole concentration in the EBL of Device B. Furthermore, Device B with an embedded PN junction features ionized acceptors in the p-AlGaN layer of the PN junction, which can deplete the electrons in the vicinity of the p-EBL and bend the conduction band upwards. It can be seen from Table 1 that the conduction band barrier height at EBL is increased from 376.4 meV in Device A to 384.2 meV in Device B, preventing the electrons from overflowing into the p-type region. Therefore, Device B exhibits a higher EQE and optical power than Device A.

In contrast, the barrier height (ΔE) at the EBL/p-$Al_{0.5}Ga_{0.5}N$ interface in Device C is decreased from 222.6 meV to 115.9 meV, allowing a significant number of holes to be injected into the EBL instead of being obstructed and reflected back to the p-type hole supplier. This can be attributed to the weakened energy band discontinuity between EBL and p-AlGaN hole supplier with optimized Al component in the p-n junction hole accelerator. It can be observed from Fig. 3(b) and (c) that energy band diagram between the EBL and p-AlGaN hole supplier is converted from a steep shape in Device B into a stepped shape in Device C. Besides, the electric field between EBL and p-AlGaN hole supplier is enhanced according to Eq. (9), which is ascribed to the increased relative dielectric constant (ε_r) decreases with a higher Al component in the AlGaN layer [50]. As shown in Fig. 3(c) and Table 1, the net work done to holes in Device C with the inserted p-$Al_{0.5}Ga_{0.5}N$/n-$Al_{0.5}Ga_{0.5}N$ structure rises from 338.1 meV to 388.5 meV, leading to an increased injection of holes into the active region. Moreover, the weakened energy band discontinuity between the EBL and p-AlGaN layer also gives rise to reduced downward bending effect of conduction band of EBL, thus increasing the Φ_C from 384.2 meV to 439.8 meV and

Optical Materials EXPRESS

suppressing the electron overflow. Consequently, the Device C with p-$Al_{0.5}Ga_{0.5}N$/n-$Al_{0.5}Ga_{0.5}N$ structure features the highest optical power and lowest efficiency droop among all devices.

With further increased AlN ratio in the insertion layer, the enhanced relative dielectric constant (ε_r) contributes to improved electric field between EBL and p-AlGaN hole supplier. However, as shown in Table 1, the kinetic energy obtained by the holes from the hole accelerator is only 261.8 meV, which is a combined effect from the neutralized the ionized donor in the n-$Al_{0.5}Ga_{0.5}N$ layer by the polarization-related negative charges and the absence of polarization-induced electric field between EBL and p-$Al_{0.6}Ga_{0.6}N$. Accordingly, the net work done to holes is redefined as

$$W_D(x) = q\int_0^L E_p dx + \int_0^{T/2} \frac{qN_A l}{\varepsilon_r\varepsilon_0} qdl + \int_{T/2}^{T} \frac{qN_D l - \sigma_2}{\varepsilon_r\varepsilon_0} qdl. \tag{12}$$

The effective valence band height of EBL is increased from 471.2 meV in Device A to 519.9 meV in Device D, resulting in a low hole concentration in the EBL. Besides, the effective conduction band height of EBL is reduced from 376.4 meV in Device A to 264.2 meV in Device D, which is driven by the disappearance of polarization-induced negative charges at p-EBL/p-$Al_{0.6}Ga_{0.4}N$ interface. Therefore, Device D exhibits the poorest optical power and the most severe efficiency droop among the investigated devices. Figure 3(f) illustrates the normalized electron and hole current density for the investigated devices at an injection current density of 150 A/cm^2. Device B and C possess lower electron leakage current in comparison with Device A, attributing to the enhanced effective conduction band barrier height for electrons (384.2 meV and 439.8 meV, respectively) at the EBL. On the contrary, because the Φ_C is decreased from 376.4 meV to 349.0 meV, the electron leakage current density of Device D is the highest among the investigated devices at an injection current density of 150 A/cm^2. Similar values for the normalized hole current density can be observed among the investigated devices, due to the same epitaxial structure of the active region and thus identical confinement from the MQWs along the flow path of the holes towards the n-type region. Some minor difference can be observed from the zoom-in curves in the inset of Fig. 3(f), in which Device C features slightly larger hole current density compared with other samples, due to the enhanced hole injection efficiency with embedded PN junctions at the p-EBL/p-AlGaN hole supplier interface.

To further verify the impact of the p-n junction hole accelerator on the device performance, we extract the carrier concentration, radiative recombination rates and non-radiative recombination rates in the MQW region at 100 A/cm^2 for the investigated devices, as shown in Fig. 4(a-c). The carrier concentration, radiative recombination rate profiles of Device A were horizontally shifted by 4 nm. Since the coupled electric field (E_{pp} and E_b) introduced by the p-n junction is capable of improving the kinetic energy of holes, Device B and Device C exhibit a higher carrier concentration in comparison with Device A without p-$Al_xGa_{1-x}N$/n-$Al_xGa_{1-x}N$ structure. Specifically, it is obvious that Device C with p-$Al_{0.5}Ga_{0.5}N$/n-$Al_{0.5}Ga_{0.5}N$ structure exhibits the highest hole concentration in the MQW region among the investigate devices. The enhanced hole concentration in Device C is attributed to not only the hole accelerator but also the reduced valence band offset between the EBL and p-AlGaN hole supplier (see Fig. 3(c)). Besides, the enhanced effective conduction barrier height (Φ_C) in Device C strengthens the capability of EBL to prevent electrons form overflowing into the p-type region. Hence, Device C possesses the highest electron concentration and radiative recombination rates as well as non-radiative recombination rates [19,51] in the MQW region among the investigated devices. However, as the AlN composition in the insertion layer increases, the carrier concentration, radiative recombination rates, and non-radiative recombination rates of Device D with p-$Al_{0.6}Ga_{0.4}N$/n-$Al_{0.6}Ga_{0.4}N$ structure are the lowest among the investigated devices, which is attributed to the reduced Φ_C and enhanced Φ_H in the EBL. In addition, we plot the I-V curves of the reference and proposed devices in Fig. 4(d) to investigate the electrical property. To illustrate the difference clearly, a zoomed-in figure for the I-V profiles is included in the inset. It can be observed that Device C presents the smallest forward voltage (V_f) at 10 A/cm^2, while Device D features the largest V_f among the investigated devices. The V_f of DUV LEDs is largely influenced by the effective barrier height for holes (Φ_H) in the EBL. As shown in Fig. 3(c), Device C exhibits the lowest Φ_H (430.8 meV) among the investigated devices, while Device D possesses the highest Φ_H (529.9 meV). Therefore, a slightly larger forward voltage is demanded for holes in Device D to overcome the potential barrier height at 10 A/cm^2.

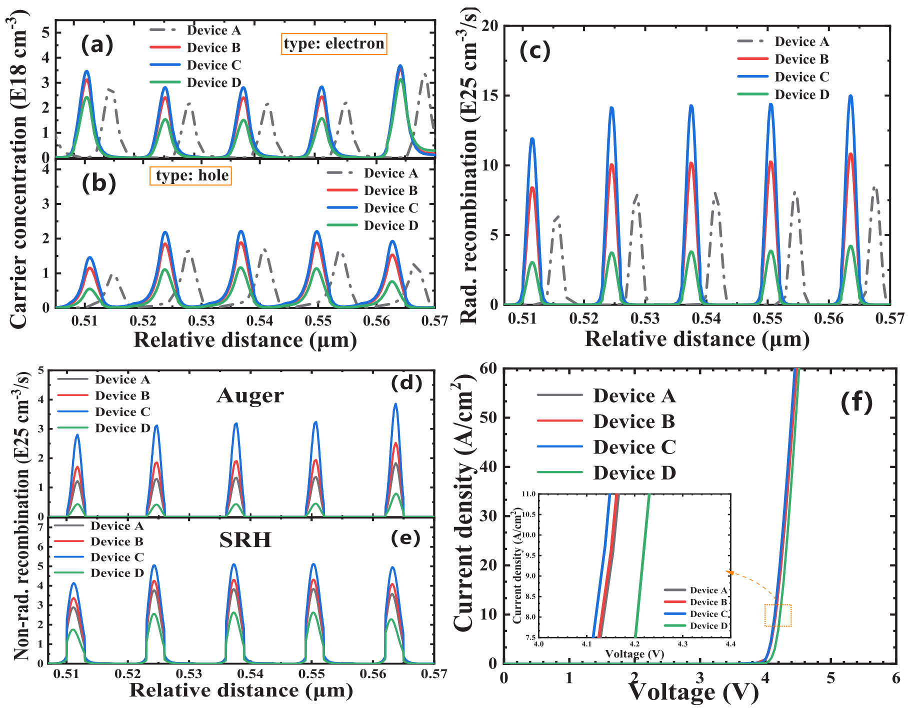

Fig. 4. (a) Electron concentration and (b) Hole concentration in MQW region at an injection current density of 100 A/cm^2 of Device A, B, C, and D. (c) Radiative recombination rates, (d) auger recombination rates, and (e) SRH recombination rates in MQW region under 100 A/cm^2 of Device A, B, C, and D. (f) IV curves for all devices.

4. Conclusion

To summarize, we propose a p-$Al_xGa_{1-x}N$/n-$Al_xGa_{1-x}N$ junction based hole accelerator to improve the hole injection efficiency of AlGaN-based DUV LEDs. A [000-1] oriented composite electric field (polarization electric field and built-in electric field) is generated between EBL and p-AlGaN hole supplier, which can enhance the kinetic energy of holes from hole supplier. By optimizing the AlN composition of p-n junction, the coupled electric field can be effectively boosted and further improve the hole injection into the active region. Besides, the barrier height at the EBL/p-AlGaN interface is decreased from 222.6 meV to 115.9 meV, ameliorating the hole blocking effect of EBL. Thus, the optical power and efficiency droop of Device C is increased by 49.4% and decreased by 76.3% at a current density of 150 A/cm^2, respectively. Therefore, the p-$Al_xGa_{1-x}N$/n-$Al_xGa_{1-x}N$ structure is promising to improve the optical performance of AlGaN-based DUV LEDs.

Funding. Shenzhen Fundamental Research Program (JCYJ20210324141212030, GJHZ20210705142537002); Guangdong Basic and Applied Basic Research Foundation (2023A1515011142, 2020A1515111018); Shandong Provincial

Optical Materials EXPRESS

Natural Science Foundation (ZR2020QF079); Scientific and Technological Plan of Guangdong Province, China (2023A0505050131); Qilu Young Scholar program (11500089963075).

Disclosures. The authors declare no conflicts of interest.

Data availability. Data underlying the results presented in this paper are not publicly available at this time but may be obtained from the authors upon reasonable request.

References

1. M. A. Khan, N. Maeda, J. Yun, M. Jo, Y. Yamada, and H. Hirayama, "Achieving 9.6% efficiency in 304 nm p-AlGaN UVB LED via increasing the holes injection and light reflectance," Sci. Rep. **12**(1), 2591 (2022).
2. T. Takano, T. Mino, J. Sakai, N. Noguchi, K. Tsubaki, and H. Hirayama, "Deep-ultraviolet light-emitting diodes with external quantum efficiency higher than 20% at 275 nm achieved by improving light-extraction efficiency," Appl. Phys. Express **10**(3), 031002 (2017).
3. M. Shatalov, W. Sun, A. Lunev, X. Hu, A. Dobrinsky, Y. Bilenko, J. Yang, M. Shur, R. Gaska, C. Moe, G. Garrett, and M. Wraback, "AlGaN Deep-Ultraviolet Light-Emitting Diodes with External Quantum Efficiency above 10%," Appl. Phys. Express **5**(8), 082101 (2012).
4. M. Ajmal Khan, E. Matsuura, Y. Kashima, and H. Hirayama, "Influence of Undoped-AlGaN Final Barrier of MQWs on the Performance of Lateral-Type UVB LEDs," Phys. Status Solidi A **216**(18), 1900185 (2019).
5. H. Hirayama, N. Maeda, S. Fujikawa, S. Toyoda, and N. Kamata, "Recent progress and future prospects of AlGaN-based high-efficiency deep-ultraviolet light-emitting diodes," Jpn. J. Appl. Phys. **53**(10), 100209 (2014).
6. R. K. Mondal, S. Adhikari, V. Chatterjee, and S. Pal, "Recent advances and challenges in AlGaN-based ultra-violet light emitting diode technologies," Mater. Res. Bull. **140**, 111258 (2021).
7. Y. Nagasawa and A. Hirano, "A Review of AlGaN-Based Deep-Ultraviolet Light-Emitting Diodes on Sapphire," Appl. Sci. **8**(8), 1264 (2018).
8. M. Usman, S. Malik, and M. Munsif, "AlGaN-based ultraviolet light-emitting diodes: challenges and opportunities," Luminescence **36**(2), 294–305 (2021).
9. Y. Yao, H. Li, M. Wang, P. Li, M. Lam, M. Iza, J. S. Speck, S. P. DenBaars, and S. Nakamura, "High external quantum efficiency (6.8%) UVA LEDs on AlN templates with quantum barrier optimization," Opt. Express **31**(18), 28649 (2023).
10. Y. Kashima, N. Maeda, E. Matsuura, M. Jo, T. Iwai, T. Morita, M. Kokubo, T. Tashiro, R. Kamimura, Y. Osada, H. Takagi, and H. Hirayama, "High external quantum efficiency (10%) AlGaN-based deep-ultraviolet light-emitting diodes achieved by using highly reflective photonic crystal on p-AlGaN contact layer," Appl. Phys. Express **11**(1), 012101 (2018).
11. Z. Guo, Z. Li, S. Lai, X. Hou, X. Fan, C. Zhong, Y. Lin, G. Chen, G. Qin, T. Gao, N. Fu, Y. Shi, X. Liao, Y. Lin, Y. Lu, W. Guo, and Z. Chen, "Investigation on external quantum efficiency droops and inactivation efficiencies of AlGaN-based ultraviolet-c LEDs at 265-285 nm," Nanotechnology **34**(33), 335201 (2023).
12. M. A. Khan, J. P. Bermundo, Y. Ishikawa, H. Ikenoue, S. Fujikawa, E. Matsuura, Y. Kashima, N. Maeda, M. Jo, and H. Hirayama, "Impact of Mg level on lattice relaxation in a p- AlGaN hole source layer and attempting excimer laser annealing on p-AlGaN HSL of UVB emitters," Nanotechnology **32**(5), 055702 (2021).
13. M. N. Sharif, M. Ajmal Khan, Q. Wali, I. Demir, F. Wang, and Y. Liu, "Performance enhancement of AlGaN deep-ultraviolet laser diode using compositional Al-grading of Si-doped layers," Opt. Laser Technol. **152**, 108156 (2022).
14. A. Khan, K. Balakrishnan, and T. Katona, "Ultraviolet light-emitting diodes based on group three nitrides," Nat. Photonics **2**(2), 77–84 (2008).
15. W. Sun, M. Shatalov, J. Deng, X. Hu, J. Yang, A. Lunev, Y. Bilenko, M. Shur, and R. Gaska, "Efficiency droop in 245-247 nm AlGaN light-emitting diodes with continuous wave 2 mW output power," Appl. Phys. Lett. **96**(6), 061102 (2010).
16. Y. Chang, M. Lai, R. Liu, S. Wang, X. Zhang, L. Zhang, Y. Lin, S. Huang, L. Chen, and R. Lin, "Efficiency Droop and Degradation in AlGaN-Based UVB Light-Emitting Diodes," Crystals **12**(8), 1082 (2022).
17. H. Murotani, R. Tanabe, K. Hisanaga, A. Hamada, K. Beppu, N. Maeda, M. A. Khan, M. Jo, H. Hirayama, and Y. Yamada, "High internal quantum efficiency and optically pumped stimulated emission in AlGaN-based UV-C multiple quantum wells," Appl. Phys. Lett. **117**(16), 162106 (2020).
18. K. Ding, V. Avrutin, Ü Özgür, and H. Morkoç, "Status of Growth of Group III-Nitride Heterostructures for Deep Ultraviolet Light-Emitting Diodes," Crystals **7**(10), 300 (2017).
19. C. Chu, K. Tian, J. Che, H. Shao, J. Kou, Y. Zhang, Z. Zhang, and H. Kuo, "On the Impact of Electron Leakage on the Efficiency Droop for AlGaN Based Deep Ultraviolet Light Emitting Diodes," IEEE Photonics J. **12**(3), 1–7 (2020).
20. Q. Wang, K. Zhang, D. Lin, X. Liang, Y. Liu, S. Zhang, H. Wu, and W. Zhao, "Introducing an n-type electron deceleration layer to enhance the luminous efficiency of AlGaN-based DUV-LEDs," Front. Phys. **11**, 1118946 (2023).
21. K. Li, N. Zeng, F. Liao, and Y. Yin, "Investigations on deep ultraviolet light-emitting diodes with quaternary AlInGaN streamlined quantum barriers for reducing polarization effect," Superlattices Microstruct. **145**, 106601 (2020).
22. C. Sheng Xia, Z. M. Simon Li, and Y. Sheng, "On the importance of AlGaN electron blocking layer design for GaN-based light-emitting diodes," Appl. Phys. Lett. **103**(23), 233505 (2013).

23. Z. Zhang, S. Huang Chen, Y. Zhang, L. Li, S. Wang, K. Tian, C. Chu, M. Fang, H. Kuo, and W. Bi, "Hole Transport Manipulation To Improve the Hole Injection for Deep Ultraviolet Light-Emitting Diodes," ACS Photonics **4**(7), 1846–1850 (2017).
24. Q. Lv, Y. Cao, R. Li, J. Liu, T. Yang, T. Mi, X. Wang, W. Liu, and J. Liu, "Performance Improvement of AlGaN-Based Deep-Ultraviolet Light-Emitting Diodes with Multigradient Electron Blocking Layer and Triangular Last Quantum Barrier," Phys. Status Solidi A **220**(13), 2300192 (2023).
25. X. Ji, J. Yan, Y. Guo, L. Sun, T. Wei, Y. Zhang, J. Wang, F. Yang, and J. Li, "Tailoring of Energy Band in Electron-Blocking Structure Enhancing the Efficiency of AlGaN-Based Deep Ultraviolet Light-Emitting Diodes," IEEE Photonics J. **8**(3), 1–7 (2016).
26. C. Chu, K. Tian, M. Fang, Y. Zhang, L. Li, W. Bi, and Z. Zhang, "On the $Al_xGa_{1-x}N/Al_yGa_{1-y}N/Al_xGa_{1-x}N$ (x > y) p-electron blocking layer to improve the hole injection for AlGaN based deep ultraviolet light-emitting diodes," Superlattices Microstruct. **113**, 472–477 (2018).
27. K. Tian, C. Chu, H. Shao, J. Che, J. Kou, M. Fang, Y. Zhang, W. Bi, and Z. Zhang, "On the polarization effect of the p-EBL/p-AlGaN/p-GaN structure for AlGaN-based deep-ultraviolet light-emitting diodes," Superlattices Microstruct. **122**, 280–285 (2018).
28. C. Chu, K. Tian, J. Che, H. Shao, J. Kou, Y. Zhang, Y. Li, M. Wang, Y. Zhu, and Z. Zhang, "On the origin of enhanced hole injection for AlGaN-based deep ultraviolet light-emitting diodes with AlN insertion layer in p-electron blocking layer," Opt. Express **27**(12), A620 (2019).
29. X. Wang, H. Sun, and Z. Guo, "Improvement of AlGaN-based deep ultraviolet light-emitting diodes by using a graded AlGaN superlattice hole reservoir layer," Opt. Mater. **86**, 133–137 (2018).
30. M. Liu, Y. Ji, H. Zhou, C. Xia, Z. Zhang, and C. Liu, "Sheet Charge Engineering Towards an Efficient Hole Injection in 290 nm Deep Ultraviolet Light-Emitting Diodes," IEEE Photonics J. **13**(4), 1–8 (2021).
31. S. Wang, Y. A. Yin, H. Gu, N. Wang, and L. Liu, "Graded AlGaN/AlGaN Superlattice Insert Layer Improved Performance of AlGaN-Based Deep Ultraviolet Light-Emitting Diodes," J. Disp. Technol. **12**(10), 1112–1116 (2016).
32. M. Liu and C. Liu, "Enhanced carrier injection in AlGaN-based deep ultraviolet light-emitting diodes by polarization engineering at the LQB/p-EBL surface," IEEE Photon. J. **14**(3), 1–5 (2021).
33. M. N. Sharif, M. I. Niass, J. J. Liou, F. Wang, and Y. Liu, "p-AlInN electron blocking layer for AlGaN-based deep-ultraviolet light-emitting diode," Superlattices Microstruct. **158**, 107022 (2021).
34. R. K. Mondal, V. Chatterjee, and S. Pal, "Effect of step-graded superlattice electron blocking layer on performance of AlGaN based deep-UV light emitting diodes," Phys. E **108**, 233–237 (2019).
35. P. Du, L. Shi, S. Liu, and S. Zhou, "High-performance AlGaN-based deep ultraviolet light-emitting diodes with different types of InAlGaN/AlGaN electron blocking layer," Jpn. J. Appl. Phys. **60**(9), 092001 (2021).
36. R. K. Mondal, V. Chatterjee, S. Prasad, and S. Pal, "Suppression of efficiency droop in AlGaN based deep UV LEDs using double side graded electron blocking layer," Semicond. Sci. Technol. **35**(5), 055031 (2020).
37. M. Ajmal Khan, N. Maeda, H. Rangaraju, M. Jo, K. Iimura, and H. Hirayama, "Efficiency droop in AlGaN crystal-based UVB LEDs in the context of electron blocking mechanism," J. Cryst. Growth **604**, 127032 (2023).
38. G. Fang, M. Zhang, and D. Xiong, "On the Near-Pole Hole Insertion Layer and the Far-Pole Hole Insertion Layer for Multi-Quantum-Well Deep Ultraviolet Light-Emitting Diodes," Nanomaterials **12**(4), 629 (2022).
39. Z. Zhang, L. Li, Y. Zhang, F. Xu, Q. Shi, B. Shen, and W. Bi, "On the electric-field reservoir for III-nitride based deep ultraviolet light-emitting diodes," Opt. Express **25**(14), 16550 (2017).
40. D. Zhang, C. Chu, K. Tian, J. Kou, W. Bi, Y. Zhang, and Z. Zhang, "Improving hole injection from p-EBL down to the end of active region by simply playing with polarization effect for AlGaN based DUV light-emitting diodes," AIP Adv. **10**(6), 65032 (2020).
41. J. Piprek, "Nitride Semiconductor Devices: Principles and Simulation," Wiley Online Books, (2007).
42. S. M. Sze, "Physics of Semiconductor Devices," Wiley Online Books, (2021).
43. D. J. H. Lambert, D. E. Lin, and R. D. Dupuis, "Simulation of the electrical characteristics of AlGaN/GaN heterojunction bipolar transistors," Solid-State Electron. **44**(2), 253–257 (2000).
44. I. Vurgaftman, J. R. Meyer, and L. R. Ram-Mohan, "Band parameters for III-V compound semiconductors and their alloys," J. Appl. Phys. **89**(11), 5815–5875 (2001).
45. Z. H. Zhang, S. T. Tan, W. Liu, Z. Ju, K. Zheng, Z. Kyaw, Y. Ji, N. Hasanov, X. W. Sun, and H. V. Demir, "Improved InGaN/GaN light-emitting diodes with a p-GaN/n-GaN/p-GaN/n-GaN/p-GaN current-spreading layer," Opt. Express **21**(4), 4958–4969 (2013).
46. [Online]. Available: http://www.crosslight.com/. Accessed:June 2019.
47. Z. Zhang, Y. Zhang, W. Bi, C. Geng, S. Xu, H. V. Demir, and X. W. Sun, "A charge inverter for III-nitride light-emitting diodes," Appl. Phys. Lett. **108**(13), 133502 (2016).
48. C. S. Xia, Z. M. Simon Li, Y. Sheng, L. W. Cheng, W. D. Hu, and W. Lu, "Simulation of InGaN/GaN light-emitting diodes with a non-local quantum well transport model," Opt. Quantum Electron. **45**(7), 597–604 (2013).
49. M. Kneissl, T. Seong, J. Han, and H. Amano, "The emergence and prospects of deep-ultraviolet light-emitting diode technologies," Nat. Photonics **13**(4), 233–244 (2019).
50. L. Li, Q. Shi, K. Tian, C. Chu, M. Fang, R. Meng, Y. Zhang, Z. Zhang, and W. Bi, "A dielectric-constant-controlled tunnel junction for III-nitride light-emitting diodes," Phys. Status Solidi A **214**(6), 1600937 (2017).

Optical Materials EXPRESS

51. H. Murotani, H. Miyoshi, R. Takeda, H. Nakao, M. Ajmal Khan, N. Maeda, M. Jo, H. Hirayama, and Y. Yamada, "Correlation between excitons recombination dynamics and internal quantum efficiency of AlGaN-based UV-A multiple quantum wells," J. Appl. Phys. **128**(10), 105704 (2020).